VIII Congresso
Ibero-americano de Acústica
acústica 2012
1-3 outubro
Évora - Portugal

ACOUSTIC SEAFLOOR CLASSIFICATION USING BACKSCATTERED LOCAL ANGULAR RESPONSES OBTAINED AT SEA.

Stelio Haniotis, Carlos A. Negreira

Instituto de Física de la Facultad de Ciencias. Igua 4225, Montevideo 11400. Uruguay.
(stelio@fisica.edu.uy, carlosn@fisica.edu.uy)

Abstract
This work addresses the acoustic classification of the marine bottom sediment in two areas of the Mediterranean Sea located near Barcelona. Data was acquired at sea with the prototype front-scan sonar COSMOS which was developed under the European MAST III program (COSMOS Project - Contract no. MAS3-CT97-0090).
Due to its frontal geometry, cosmos sonar can measure the local angular dependence of the backscattered strength over a large angular domain. Multilayered mosaic images were built and thus, each pixel was associated with a set of backscattered intensity values (one for each angle of view).
In a previous work, the local angular response (LAR) of seafloor reverberation has been classified; each classed response has been projected on a map, so a segmentation map of the surveyed zones was obtained. In this paper, the integral scattering model is applied for geo-acoustic inversion, on the classed LAR. The inversion process is performed by fitting a set of input parameters for each class, which minimizes the difference between the model angular responses and the measured LAR curve. Each set of parameters is linked with a type of sediment by means a lookup table, so that the classification can be obtained. Finally, the comparison of classification with ground truth data is performed.
Keywords: seabed classification, geo-acoustic inversion, angular backscattering, underwater acoustic.

PACS no. 43.30.Pc, 43.30.Hw

1 Introduction

The utilization of remote acoustic techniques for seafloor classification is an alternative to mechanical sampling and probing methods. These direct methods are accurate but consume a lot of time and the spatial sampling of the surveyed areas is very sparse. The efforts of recent decades tend to lean towards the automatic segmentation and the classification of the seabed by remote acoustic methods.

When data is presented in the form of backscatter images obtained by sonar, image processing techniques are generally used for segmentation. The seafloor classification is then done by empirical methods [1]-[5]. Data acquired with single-beam echosounder are also used for seafloor classification, [6]-[10].

Another way of approaching the problem comes when the angular backscatter response of seafloor is known. The angular response depends on both the upper morphology of the seabed such as the roughness of the water/sediment interface and the volume of the structure of the sediment. This

dependency is exploited to classify the seafloor. Several studies have been carried out either directly by exploiting the angular response [11]-[18] as well as using the fact that backscatter statistics strongly depend on the incidence angle [19]-[22].

In this paper, classification of seafloor sediments is achieved by exploiting the angular responses backscattered by the seafloor. Data was acquired with the prototype front-scan sonar COSMOS, developed within the European MAST III program (COSMOS Project - Contract no. MAS3-CT97-0090). Unlike conventional systems that scan the seafloor along successive bands in the cross-track direction [23][24], the COSMOS system emits the sound forwards [25]. Thanks to the forward geometry (Figure 1), fixed points of the seafloor are repeatedly insonified under different view angles while the sonar is moving forward. This overlap provides the ability to map out the local angular dependence of the backscattered strength. In a previous paper [26], backscatter images were constructed and for each pixel a set of *n* intensity values were associated (one value for each angle of view). Thus, the local angular response (LAR) of each point (pixel) of the bottom is available. Then LAR were classified via the clusters identification process in a principal component space [27]. In this paper, the integral scattering model APL-UW[1] [28] is applied for geo-acoustic inversion on classed LAR. The inversion process is performed by fitting a set of input parameters for each class, which minimizes the difference between the APL model angular responses and the measured LAR curve. Each set of parameters are linked with a type of sediment via a lookup table, the classification is then obtained. Finally, the class of sediment obtained for each class is compared with the samples taken during the COSMOS campaign in question, previous campaigns and maps.

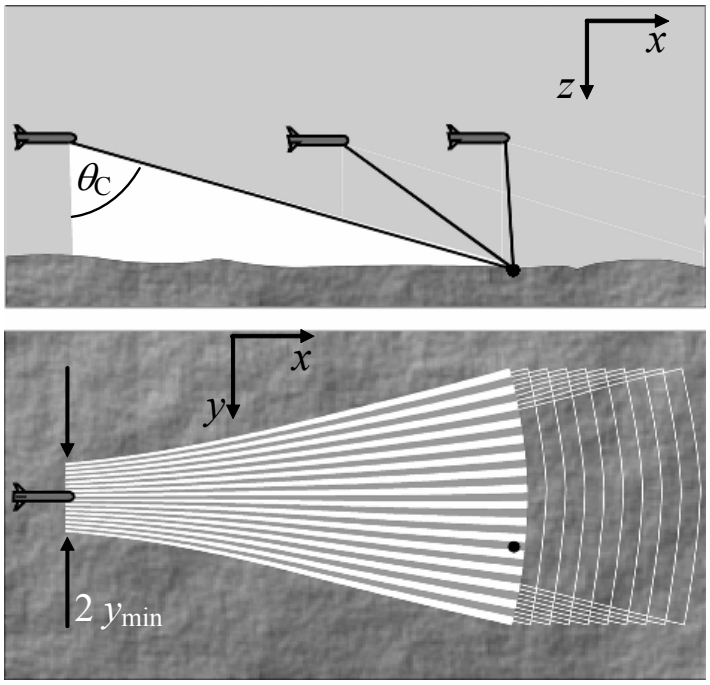

Figure 1 – Cosmos sonar beampatern

[1] Applied Physics Laboratory-University of Washington

2 Acquisition system

COSMOS is a prototype multibeam sonar system designed for the imaging, bathymetric measurements and characterization of the seafloor which work at a central frequency of 100 kHz. The main feature of the system is the frontal acquisition geometry, which lets obtain multiple viewing angles due to the overlap of scanned sectors during successive pings.

The maximum slant range is a few hundred meters and the solid angle covered by the acoustic beams has an aperture larger than θ_C= 80° in site (Figure 1), starting from near nadir to near horizontal. The aperture in azimuth is 25º. With this design, a large coverage for the backscatter angular responses of the seafloor is obtained, over the along-track central band that is surveyed. This central band has a width of about $2y_{min}$=0.4H, where H is the depth (Figure 1).

The emitter antenna consists of an arc of a circle, 80 cm long and 1.4 m radius. The plane of the circle is slanted 40° below the horizontal. The measured source level is 207 dB re 1 μPa rms @ 1m. The receiving are two parallel linear arrays in order to allow beam forming in the azimuth and the interferometric measurements (site angle). The boresight direction of the receiving antenna is slanted 40° below the horizontal like the transmitting. Each array has 32 elements with a pitch of 22.5 mm and each one is 72 cm long. This geometry gives an angular resolution in azimuth of approximately 1.5º (at −3 dB) in the band around 100 kHz. The formation of 31 beams is then sufficient to fully cover the total aperture in azimuth.

The transmitted signal is a chirp, whose amplitude is shaded by a truncated Gaussian window (20% of the max amplitude at the ends). The bandwidth is B = 3 kHz and the Chirp duration is 8 ms. Therefore, the echographic radial resolution $\delta r \approx c/(2B)$ obtained after pulse compression is about 25 cm. A comprehensive description of the COSMOS system can be found in [26][29].

3 Studied areas

Data was acquired in the Mediterranean Sea off the coast of Barcelona, in the Blanes and Besos regions. The zone has a wide variety of bottom sedimentary characteristics which are relatively well known.

The area in which Besos is located is near the river-mouth of the Besos River within the rectangle: 41°25' N - 41°22' N; 2°14' E - 2°19' E. In the campaign they traveled 34 km with depths varying between 25 m and 60 m. For the study, the area is divided into three regions: East-Besos (EB) Central-Besos (CB) and West-Besos (WB) (Figure 3). The EB region is the deepest of them (45 to 60 m). It has soft sediment, and presents a well-defined sand body. The CB region has very varied sediments with subtle transitions. It is characterized by a large area of anthropogenic sediment due to the sewer emissions, and a region of abrasion resulting from the effects of fishing activities. The WB region has a soft and uniform relief whose main interest is the presence of a pipeline.

The Blanes area is located within 41°41' N - 41°39' N; 2°47' E - 2°50' E. It was surveyed in 14 transects with a total distance of 25 km covered, the depth varying between 15 and 55 m. The background is diverse, consisting of sandy gravel and rock deposits, with abrupt transitions (Figure 2).

Grab and core samples in the vicinity of the sonar survey were taken both in the Besos and Blanes area (Figure 2 and 3). These samples together with other samples taken in a previous survey were used to the ground truth.

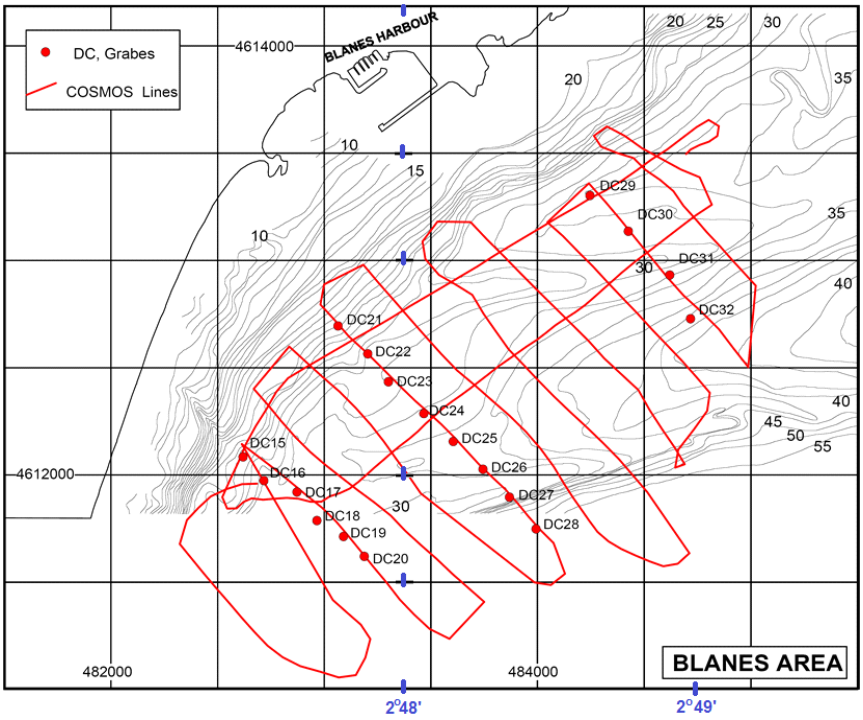

Figure 2 – Bathymetric map (in meters) showing the location of COSMOS lines, and sediment samples (DC, grabs) in the Blanes area

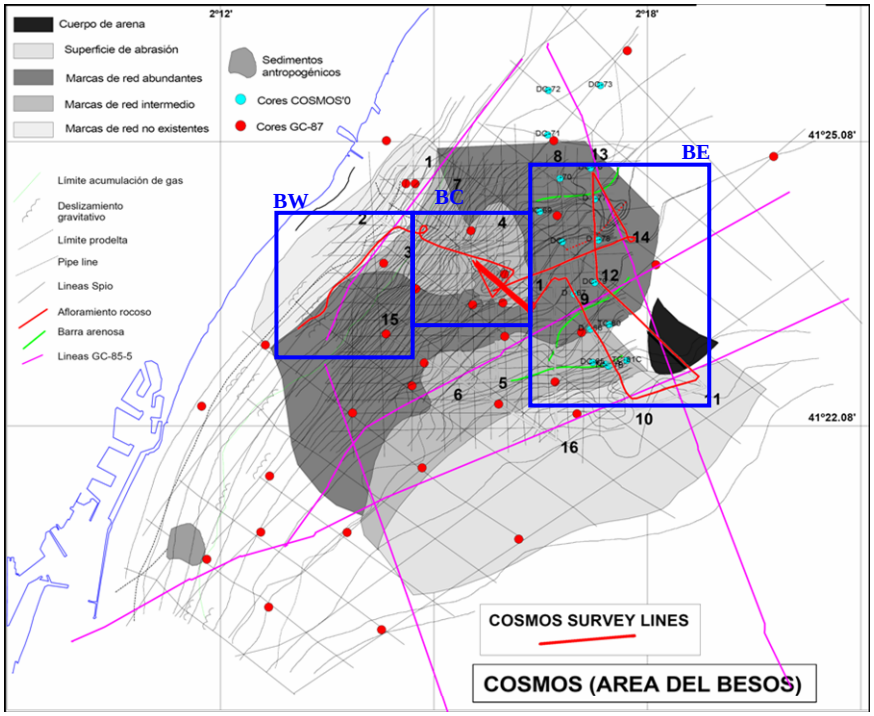

Figure 3 – Besos region. In red: transects followed during the campaign. The blue points indicate the sampling carried out during COSMOS survey. The red dots show the locations of samples taken in 1987.

4 Data pre-processing

Raw transducer data was processed in order to build a set of beamformed data that takes into account the calibration parameters. For each ping the altitude of the antennae is estimated using to the first bottom return delay. The bottom is assumed to be locally a horizontal plane for mapping the beamformed acoustic data. Both the Doppler effect and refraction are neglected due to the small water gradient temperature and the low speed of the vessel (3 knots).

As a result of the multiple viewing angles, the acoustic data are sorted into a multi-layered map, each layer corresponding to a small range of grazing angles. Therefore, each layer provides a backscatter image of the bottom seen under a restricted range of grazing angle. The contributions of the layers are weighted to account the different cell resolution of each grazing angle. A detailed description of the parameter calibration, beam-forming process and multi-layered image can be found in [26][30].

Finally, to be able to group the LAR backscattered according to a limited number of classes, a principal component analysis (PCA) of the responses is performed [31]. Acoustic data is sorted into a matrix $\mathbf{X} = \left[x_{i,j} \right]$ $i = 1, \ldots p$ and $j = 1,\ldots,n$), with p rows (pixels) and n columns (angles of view). The range of grazing angles is divided into n=24 angular bins within the interval [14º, 69°]. Each element $x_{i,j}$ of $\mathbf{X}$ represents the intensity that is backscattered by the pixel #i seen under the grazing angle γ_j. The matrix $\mathbf{X}$ is converted into the logarithmic scale (dB), and then rescaled at a zero mean and unit variance to build a matrix $\mathbf{Z}$. The correlation matrix $\mathbf{C} = \mathbf{Z}^T\mathbf{Z}$ is computed; its eigenvalues and eigenvectors are then found. After this, the columns of the Z matrix are projected on the first three eigenvectors base and clusters are identified to define classes. The barycenter of each cluster is determined and returned to their original data space (performing an inverse PCA process). These centers give the typical angular backscatter responses associated with each class.

A total of seven types of responses were classified (Figure 4) from soils with very high reflectivity (Class # 1-yellow) to "soft bottom" (# 6 brown). Finally, a segmentation map is built for each studied area (Blanes, EB, CB and WB) in assigning to each geo-referenced pixel, the class that it had in the PC space. Figures 5 and 6 show the segmentation maps superimposed on the backscatter image in the Blanes and BC area, where each color corresponds to a class. Particularly, the Blanes area shows a clear coincidence between segmentation and the changes in the image texture.

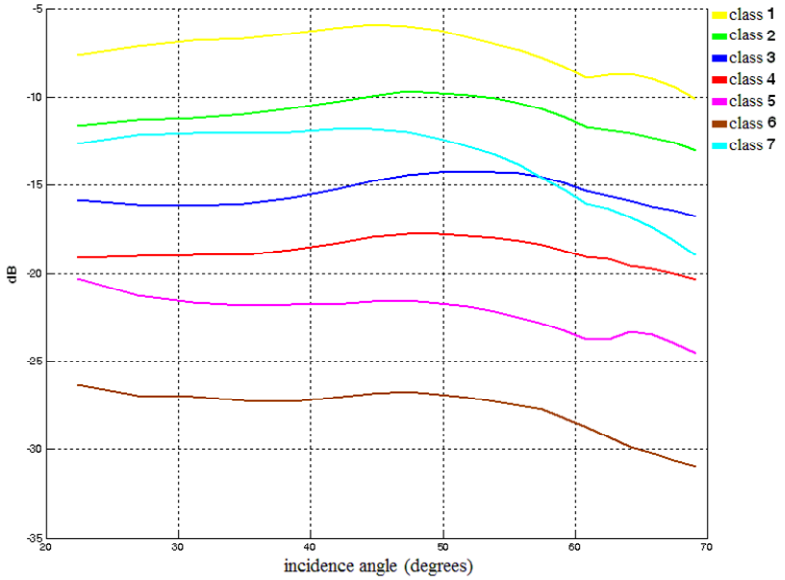

Figure 4 Angular responses by classes

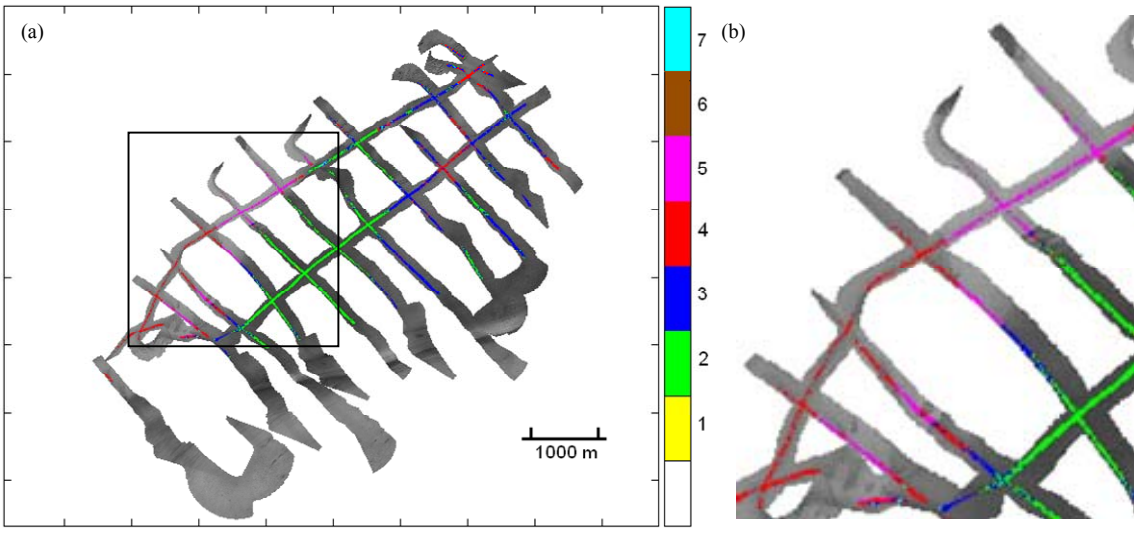

Figura 5 – Blanes Zone. (a) Classes map superimposed to the backscattering image. (b) Detail

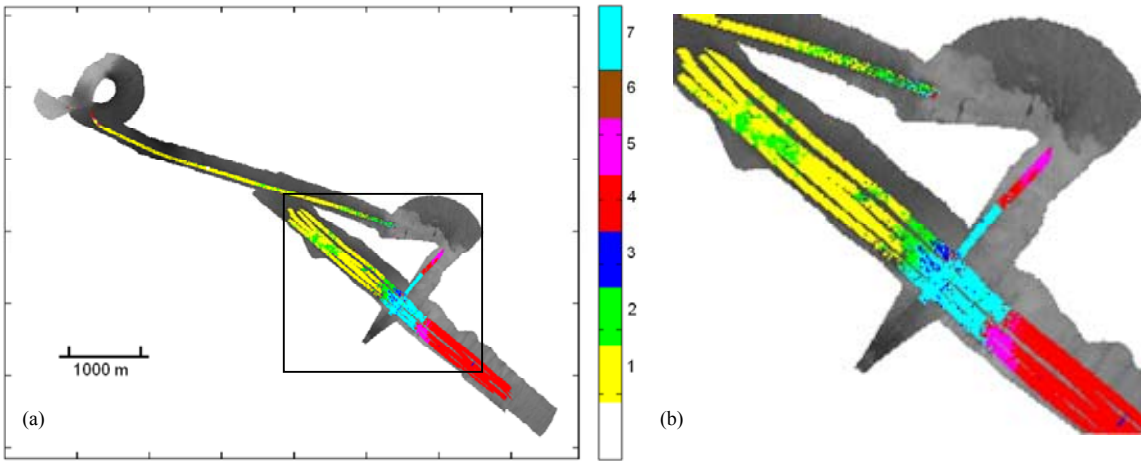

Figure 6 – (a) Central-Besos Area. Class map superimposed on the backscattering image. (b) Detail

5 The Model

Fluid sediment models that predict scattering from both the roughness of the seafloor surface and variations in sediment sound speed and density have proven to be accurate predictors of the backscattering strengths measured in several experiments [32][33][34].

The APL_UW backscattering strength model [28] is applicable over the frequency interval 10 - 100 kHz. The sediment is modelled as a simple, semi-infinite fluid which is assumed to be statistically homogeneous both in the horizontal and in the vertical. Layering and gradients are not included. Volume backscattering contributions are parameterized by an equivalent surface backscatter. It is assumed that the two-dimensional relief spectrum is isotropic and obeys the power law $W(\mathbf{K}) = w_2 (h_0 K)^{-g_2}$. In this equation, K is the wavenumber of bottom relief features;

$K = 2p/\mathrm{L}$ where Λ is the associated wavelength and h_0 is a reference length equal to 1 cm. Furthermore, the model requires six input parameters defined in Table 1.

At incident angle θ, bottom backscattering strength $BS(\theta)$ is the decibel equivalent of the scattering cross section [35], which is broken into two parts:

$$BS(q) = 10\log_{10}\left(s_r(q) + s_v(q)\right) \tag{1}$$

Where, σ_r (θ) is the dimensionless backscattering cross section per unit solid angle per unit area due to interface roughness; $\sigma_v(\theta)$ is the dimensionless backscattering cross section due to volume scattering from below the interface.

Three different approximations are used for roughness scattering cross section $\sigma_r(\theta)$. For smooth and moderately rough bottom (e. g. clay, silt and sand), σ_r is computed using the Kirchhoff approximation [36] for grazing angles near 90º and the composite roughness approximation [37][38] is used for all other angles. For rough bottom (e. g., gravel and rock) an empirical expression taken from [39] is used.

For sediment volume scattering $\sigma_v(\theta)$ including refraction and transmission loss at the sediment-water interface, an expression published in [40] is used. This expression is generalized to allow the effect of the absorption of the transmission coefficient of the sediment/water interface and incorporate shadowing and bottom slope corrections.

Table 1 – Inputs parameters used in de bottom backscattering strength model.

Symbol	Definition	Short name
ρ	Ratio of sediment mass density to water mass density	Density ratio
v	Ratio of sediment sound speed to water sound speed	Sound speed ratio
δ	Ratio of imaginary wavenumber to real wavenumber for the sediment	Loss parameter
σ_2	Ratio of sediment volume scattering cross-section to sediment attenuation coefficient	Volume parameter
γ_2	Exponent of bottom relief spectrum	Spectral exponent
w_2	Strength of bottom relief spectrum (cm^4) at wavenumber $2\pi/\lambda$ cm^{-1}	Spectral strength

6 Inversion scheme

At the end of the segmentation process, a class and a spatial geo-referenced coordinate is linked to every pixel. In addition, each pixel has a LAR associated with it. From these coordinates, the intensity backscattered by pixels belonging to the same segment are read and evaluated. The mean LAR in linear scale is computed for each class and then the response is finally transformed to decibels. For each of the seven responses classed an inversion scheme is performed. The problem that occurs is finding the set of input parameters of Table 1 that best fits the given data set. That is, which set of parameters minimizes the difference between the $BS(\theta)$ model curve and the measured $BS(\theta)$ data. So, for each class (from 1 to 7) we minimize the cost function.

$$S_k(\mathbf{p}) = \sum_{i=1}^{26}\left(BS(q_i) - \hat{BS}(q_i,\mathbf{p})\right)^2 \quad k = 1,\cdots 7 \tag{2}$$

$\hat{BS}(\theta_i)$ and $BS(\theta_i)$ are the backscattering strength at the incidence θ_i measured and modelled respectively and $\mathbf{p} = [\rho, v, \delta, \sigma_2, \gamma_2, w_2]$ is the vector of parameter. After the process we obtain a vector $\mathbf{p_k}$ (k = 1 … 7) of parameters for every class.

The sum of the squares of the data deviations from the model prediction are used as a measure of goodness of the fit. It is then evaluated.

$$D_k = \sqrt{\frac{1}{26}\sum_{i=1}^{26}\left[BS(q_i) - \hat{BS}(q_i, \mathbf{p}_k)\right]^2} \quad k = 1, \cdots, 7 \tag{3}$$

For the parameter γ_2 (spectral exponent) we have used a fixed value of 3.25 according to the recommendation given in [28]. The ranges of the input parameter used are presented in Table 2

Table 2 – limits of the input parameters

Parameter	Range
ρ	1.00 – 3.00
ν	0.800 – 3.00
δ	0.00 – 0.100
σ_2	0.00 – 0.500
w_2	0.00 – 1.00 (cm^4)

7 Result

Table 3 shows, for each class, the input parameters that best fit into the minimization process of the cost function (2). The adjustment was made by putting into consideration that between the two adjacent BS curves, the minimum difference is about 3 dB (Figure 4). As a result of this, a dispersion (Δ) of about 0.5 dB was considered acceptable.

Table 3 – Best fitted parameters and their dispersion

class	ρ	ν	δ	σ_2	w(cm^4)	Δ (dB)
# 1	1.35	1.29	0.0001	0.0028	0.1656	0.31
# 2	2.49	1.78	0.0140	0.0007	0.0610	0.56
# 3	2.44	1.36	0.0170	0.0010	0.0480	0.56
# 4	1.67	1.16	0.0100	0.0055	0.059	0.34
# 5	1.44	1.06	0.0150	0.0039	0.0015	0.46
# 6	1.15	1.09	0.0700	0.0010	0.0005	0.47
# 7	1.35	1.19	0.0240	0.0252	0.0040	0.44

Each set of parameters of Table 3 is identified with a sediment type. This identification process is carried out in the table given in [28]. The table relates standard sediment types to model parameters. The sediment name is assumed to be the name appropriate to the bulk of sediment, rather than superficial sediment. The sediment names are taken from the classification scheme given in [41] [42] [43] [44].

A summary table of class analysis is given in Table 4. When available, the ground truth column shows the granulometry from COSMOS cruise samples analysis [45]. Otherwise, the data is taken from ICM[2] data and maps [46]. Class 1 cannot be identified with any sediment from the UW-APL table. Maps indicate that this area is a large anthropogenic sediment deposit of sewer emissions. Class 7 has not been identified either as the attenuation parameter set is 10 times higher than normal for the type of sediment identified with the other parameters of the same class.The other parameters fits well within a narrow range of sediment types and they are easily identified. In particular, the shells that were found in areas affected by the class # 4 explain the high roughness.

[2] l'Institut de Ciències del Mar, Barcelona. España.

Table 4 – Classification table and Ground truth

Class	Classification (via lookup table UW-APL)	Ground truth			
		Gravel	Sand	Silt	Clay
1	without identification	anthropogenic sediment			
2	Cobble - gravel - pebble / Sandy gravel, close to rocky roughness.	23%	73%	4%	-
3	Sandy gravel / Very coarse sand	14%	84%	2%	-
4	Medium sand / Muddy gravel; with greater than normal roughness.	Turritellas and bivalves (within BE)			
		1%	65%	24%	9%
5	Fine sand-silty sand / Muddy sand / Very fine sand	-	96%	4 %	-
		Soft and homogeneous bottom			
6	Medium silt, sand-silt-clay	brown mud-grey mud			
7	Gravely muddy sand / Medium sand / Muddy gravel/Fine sand – silty sand. Volume parameter × 10	Abundant Trawling marks. Erosive plataform			

8 Conclusions

This work shows the acoustic seabed classification by exploiting data obtained with the prototype sonar COSMOS. The frontal architecture of the system allows us to obtain the local angular response from the bottom of the seabed. Thus, the system is especially adapted for seafloor characterization.
In previous work, seven types of responses acquired with COSMOS were classified. In this article these responses were identified with a type of sediment and a classification of the seafloor was performed.

Both in Blanes (abrupt transitions) as Besos (subtle transitions), the classification displayed a strong correlation, with the available information, about the nature of the seabed in classes #2 to #6.
The class #7 has been successfully classified regarding the sediment composition. However, taking into account the factor 10 in the volume parameter, it is not possible to identify any sediment within a band of reasonable variability. This is understandable because in the area where the class #7 is located, the results correspond to an abrasion platform with significant trawling marks. This gives special characteristics to the bottom that are not considered in a table of standard sediments. However, this area has been correctly discriminated by the segmentation procedure. Similarly, the class #1 area has been well insulated but it was not possible to identify the sediment, since it corresponds to human waste. It is necessary to extend the model to classify these cases.

To summarise, the procedure used for remote acoustic classification of the seabed is satisfactory and it can be improved by a model that includes atypical bottoms. In addition, all discriminated bottom patches correspond to sediments with very different compositions. Thus both the segmentation method and the performance of COSMOS for sea floor classification are validated.

Acknowledgements

The authors wish to thank P. Cervenka (Institut Jean Le Rond d'Alembert, France) for his collaboration during the development of the thesis that led to this article.

References

[1] Brown, C.; Todd, B.J.; Kostylev, V.E.; Pickrill, R.A. Image-based classification of multibeam sonar backscatter data for objective surficial sediment mapping of Georges Bank, Canadañ. *Cont. Shelf Res*., Vol. 31, 2011, pp.110–119.

[2] Blondel, Ph.; Gómez Sichi, O. Textural analyses of multibeam sonar imagery from Stanton Banks, Northern Ireland continental shelf, *Appl. Acous*., Vol. 70, 2009, pp. 1288–1297.

[3] Karoui I.; Fablet R.; Boucher J.; Augustin J.M. Seabed segmentation using optimized statistics of sonar textures. *IEEE Trans. Geosci. Remote Sens.*, Vol. 47 (6), 2009, pp. 1621–1631.

[4] Pican N.; Trucco E.; Ross M.; Lane D.M.; Petillot Y.; Tena Ruiz I. Texture analysis for seabed classification: Co-occurrence Matrices vs self-organizing maps. *Proc. IEEE/OES OCEANS' 98 vol. 1*, Nice, 28 Sep-1 Oct 1998, 424–428.

[5] Blondel Ph. Textural Analysis of Sidescan Sonar Imagery and Generic Seafloor Characterization, *J. Acoust. Soc. Am.* Vol. 105, 1999, pp. 1206-1206.

[6] Pouliquen, E.; Lurton, X. Sea-bed identification using echosounder signal. *European Conference on Underwater Acoustics*, Elsevier Applied Science, London and New York, 1992, 535.

[7] Pouliquen, E.; Lurton, X. Identification de la nature du fond de la mer a l'aide de signaux d'échos-sondeurs: I. Modélisation d'échos réverbérés par le fond. *Acta Acustica* Vol. 2 (2), 1994, pp. 113-126.

[8] Sternlicht, D.; de Moustier C. Time-dependent seafloor acoustic backscatter (10–100 kHz). *J. Acoust. Soc. Am.* Vol. 114 (5), 2003, pp. 2709-2725.

[9] van Walree, P. A.; Ainslie, M. A.; Simons, D. G. Mean grain size mapping with single-beam echo sounders. *J. Acoust. Soc. Am.* Vol. 120 (5) 2006, pp. 2555-2566

[10] Amiri-Simkooei, R.; Snellen, M.; Simons, D. G. Principal Component Analysis of Single-Beam Echo-Sounder Signal Features for Seafloor Classification. *IEEE J. Ocean. Eng.* Vol. 36 (2), 2011, pp. 259 – 272.

[11] Hughes-Clarke, J.E.; Danforth, B.W.; Valentine P. Areal Seabed Classification using Backscatter Angular Response at 95kHz. *NATO SACLANTCEN Conference Proceedings Series CP-45, High Frequency Acoustics in Shallow Water*, La Spezia, Italy, June 1997, pp.243-250.

[12] Hughes-Clarke J.E. Toward remote classification using the angular response of acoustic backscattering: a case study from multiple overlapping GLORIA data. *IEEE J. Ocean. Eng.*, Vol.19 (1), 1994, pp. 112-127.

[13] Fonseca L.; Brown C.J.; Calder B.; Mayer L.; Rzhanov Y. Angular range analysis of acoustic themes from Stanton Banks Ireland: A link between visual interpretation and multibeam echosounder angular signatures. *Appl. Acoust.*, Vol. 70, 2009, pp. 1298–1304.

[14] de Moustier C.; Alexandrou D. Angular dependence of 12 kHz seafloor acoustic backscatter. *J. Acoust. Soc. Am.*, Vol. 90 (1), 1991, pp. 522-531.

[15] Hamilton L.J.; Parnum I. Acoustic seabed segmentation from direct statistical clustering of entire multibeam sonar backscatter curves. *Cont. Shelf Res*., Vol. 31, 2011, pp. 138–148.

[16] Fonseca L.; Mayer L. Remote estimation of surficial seafloor properties through the application Angular Range Analysis to multibeam sonar data. *Mar. Geophys Res*., Vol. 28, 2007, pp. 119–126.

[17] Chakraborty B.; Kodagali V.; Baracho J. Sea-floor classification using Multibeam Echo-Sounding angular backscatter data: A real-time approach employing hybrid neural network architecture. *IEEE J. Ocean. Eng.*, Vol. 28 (1), 2003, pp. 121-128.

[18] Haris, K.; Chakraborty, B.; Chanchal De; Prabhudesai, R. G.; Fernandes, W. Model-based seafloor characterization employing multi-beam angular backscatter data—A comparative study with dual-frequency single beam, *J. Acoust. Soc. Am.* Vol. 130 (6), 2011, pp. 3623-3632.

[19] Hellequin, L.; Boucher, J.; Lurton, X. Processing of high frequency multibeam echosounder data for seafloor characterization. *IEEE J. Ocean. Eng*., Vol. 28 (1), 2003, pp. 78–89.

[20] Lyons, A.; Abraham, D. Statistical characterization of high-frequency shallow-water sea-floor backscatter. *J. Acoust. Soc. Amer.*, Vol. 106 (3), 1999, pp. 1307–1315.

[21] Le Chenadec, G. Analyse de descripteurs énergétiques et statistiques pour la caractérisation des fonds marins. *Ph.D. dissertation*, Univ. De Bretagne Occidentale, Brest, France, 2004.

[22] Le Chenadec, G.; Boucher, J.; Lurton, X. Angular Dependence of K-Distributed Sonar Data. *IEEE Transactions on Geoscience and Remote Sensing*, Vol. 45 (5), 2007, pp. 1224-1235.

[23] de Moustier, C. State of the art in swath bathymetry survey systems. *Int. Hydro. Rev.*, Vol. 65, 1988, pp. 25-54.

[24] de Moustier, C.; Malsumoto H. Seafloor acoustic remote sensing with multibeam echosounders and bathymetric sidescan sonar systems. *Mar. Geophys. Res.*, Vol. 15, 1993, pp. 27-42.

[25] Cervenka, P. Characterization and observation of de sea-floor with a new multibeam front-scan sonar system (COSMOS). *Proc 3rd European Marine Science and Technology Conference*, *vol. III*, Lisbon 23-27 May 1998 pp.1287-1297.

[26] Cervenka, P.; Marchal, J., Imaging with a new multi-look front-scan sonar system. *Acta Acustica*, Vol. 90, 2004, pp. 38-48.

[27] Cervenka, P.; Marchal, J. Classification of angular backscattered responses obtained at sea with a forward looking sonar system. *J. Acoust. Soc. Am.* Vol. 123 (5), 2008, 3895-3895.

[28] APL-UW; High-Frequency Ocean Environmental Acoustics Models Handbook (No. APL-UW TR 9407) Applied Physics Laboratory, University of Washington, Seattle, WA, 1994.

[29] Cervenka, P. Characterization and observation of the seafloor with a new multi-beam front-scan sonar system; Final report on Hardware Development; Université Pierre et Marie Curie, Laboratoire de Mécanique Physique (CNRS UPRESA 7068), 2003

[30] Cervenka, P. Characterization and observation of the seafloor with a new multi-beam front-scan sonar system; Final report on Data Alignmen-Imaging and Interferometry- Bathymetry) Université Pierre et Marie Curie, Laboratoire de Mécanique Physique (CNRS UPRESA 7068) 2003.

[31] Haniotis, S. Interactions ondes acoustiques / sediments marins: Application a la caracterisation des fonds. Thèse de doctorat de l'Université Pierre et Marie Curie, Paris, 2010.

[32] Jackson, D. R.; Briggs, K. B.; Williams, K. L.; Richardson, M. D. Tests of models for high-frequency seafloor backscatter. *IEEE J. Ocean. Eng*., Vol. 21, 1996, pp. 458–470.

[33] Williams, K. L.; Jackson, D. R. Bistatic bottom scattering: Model, experiments and model / data comparison. *J. Acoust. Soc. Amer*. Vol. 103(1), 1998, pp. 169–181.

[34] Williams, K. L.; Jackson, D. R.; Thorsos, E. I.; Tang, D.; Briggs, K. B. Acoustic Backscattering Experiments in a Well Characterized Sand Sediment: Data/Model Comparisons Using Sediment Fluid and Biot Models. *IEEE J. Ocean. Eng*., Vol. 27, 2002, pp. 376-387.

[35] Urick, R. J. Principles of underwater sound. McGraw-Hill, New York, 1983.

[36] Ishimaru, A. Wave Propagation and Scattering in Random Media; Volume II: Multiple scattering, turbulence, rough surfaces and remote sensing, Academic Press, New York, 1978.

[37] McDaniel, S.T.; Gorman, A.D. An examination of the composite-roughness scattering model. *J Acoust Soc Am.* Vol. 73, 1983, pp. 1476-1486.

[38] Jackson, D. R.; Winebrenner, D. P.; Ishamaru, A. Application of the composite roughness model to high-frequency bottom backscattering. *J. Acoust. Soc. Amer.,* Vol. 79(5), 1986, pp. 1410–1422.

[39] Jackson, D. R. Third Report on TTCP bottom scattering measurement: model development, APL-UW 8708. September 1987.

[40] Stockhausen, J. H. Scattering from the volume of an inhomogeneous half-space. Report No. 63/9, Naval Research Establishment, Canada, 1963.

[41] Wentworth, C.K. A scale of grade and class for elastic sediments. *J. Geology*. Vol. 30, 1922, pp. 377-392.

[42] Lane, E.W. Report of the committee on sedimentary terminology, *Trans AGU*. 289, 1947, pp. 936-938.

[43] Shepard F.P. Nomenclature based on sand-silt-clay ratios. *J. Sediment petrol*. Vol. 24, 1954, pp. 151-158.

[44] Folk R.L., The distinction between grain zise and mineral composition in sedimentary-rock nomenclature. J. Geology, 62, 1954, 344-359.

[45] ICM COSMOS report, Characterization and observation of the seafloor with a new multi-beam front-scan sonar system; Final report on Research Cruise Reports& ROSCOP, Institut de Ciències del Mar. CSIC, Barcelona March 2001

[46] Departament de Geologia Marina de l'Institut de Ciències del Mar (ICM), Barcelona. http://www.icm.csic.es/geo/gma/SurveyMaps/